

# Multi-Frequency Joint Community Detection and Phase Synchronization

Lingda Wang, and Zhizhen Zhao

*Coordinated Science Laboratory, and Department of Electrical and Computer Engineering  
University of Illinois at Urbana-Champaign  
{lingdaw2, zhizhenz}@illinois.edu*

June 27, 2022

## Abstract

This paper studies the joint community detection and phase synchronization problem on the *stochastic block model with relative phase*, where each node is associated with a phase. This problem, with a variety of real-world applications, aims to recover community memberships and associated phases simultaneously. By studying the maximum likelihood estimation formulation, we show that this problem exhibits a “*multi-frequency*” structure. To this end, two simple yet efficient algorithms that leverage information across multiple frequencies are proposed. The former is a spectral method based on the novel multi-frequency column-pivoted QR factorization, and the latter is an iterative multi-frequency generalized power method. Numerical experiments indicate our proposed algorithms outperform state-of-the-art algorithms, in recovering community memberships and associated phases.

## 1 Introduction

*Community detection on stochastic block model* (SBM) (Abbe, 2017), and *phase synchronization* (Singer, 2011), are both of fundamental importance across multiple fields, such as machine learning (Chen et al., 2017), social science (Girvan and Newman, 2002), and signal processing (Singer et al., 2011; Zhao and Singer, 2014), to name a few.

**Community detection on SBM.** Consider the symmetric SBM with  $N$  nodes that fall into  $M$  underlying communities of equal size  $s = N/M$ . SBM generates a random graph  $\mathcal{G}$  such that each pair of nodes  $(i, j)$  are connected independently with probability  $p$  if  $(i, j)$  belong to the same community, and with probability  $q$  otherwise. The goal is to recover underlying community memberships of nodes given the adjacency matrix  $A_{\text{SBM}} \in \{0, 1\}^{N \times N}$  of the observed graph  $\mathcal{G}$ . During the past decade, significant progress has been made on the information-theoretic threshold of the exact recovery on SBM (Abbe et al., 2015; Abbe and Sandon, 2015; Abbe, 2017), in the regime  $p, q = \mathcal{O}(\log N/N)$ . The maximum likelihood estimation (MLE) formulation of community detection on SBM,

$$\max_{\mathbf{H} \in \mathcal{H}} \langle \mathbf{A}_{\text{SBM}}, \mathbf{H} \mathbf{H}^\top \rangle, \quad \text{with } \mathcal{H} := \{ \mathbf{H} \in \{0, 1\}^{N \times M} : \mathbf{H} \mathbf{1}_M = \mathbf{1}_N, \mathbf{H}^\top \mathbf{1}_N = s \mathbf{1}_M \}, \quad (1)$$

is capable of achieving the exact recovery at the above regime. However, obtaining the maximum likelihood estimator of (1) is non-convex and NP-hard in the worst case. Therefore, different approaches based on MLE (1) or others are proposed to tackle this problem, such as the spectral method (Abbe et al., 2020; Krzakala et al., 2013; Massoulié, 2014; Ng et al., 2001; Vu, 2018; Yun and Proutiere, 2014; Su et al., 2019; McSherry, 2001), semidefinite programming (SDP) (Abbe et al., 2015; Amini and Levina, 2018; Bandeira, 2018; Guédon and Vershynin, 2016; Hajek et al., 2016a,b; Perry and Wein, 2017; Fei and Chen, 2018; Li et al., 2021), and belief propagation (Abbe and Sandon, 2015; Decelle et al., 2011).

**Phase Synchronization.** The phase synchronization problem concerns recovering phase angles  $\theta_1, \dots, \theta_N$  in  $[0, 2\pi)$  from a subset of possibly noisy phase transitions  $\theta_{ij} := (\theta_i - \theta_j) \bmod 2\pi$ . The phase synchronization problem can be encoded into an observation graph  $\mathcal{G}$ , where each phase is associated with a node  $i$  and the phase transitions are observed between  $\theta_i$  and  $\theta_j$  if and only if there is an edge in  $\mathcal{G}$  connecting the pair of nodes  $(i, j)$ .

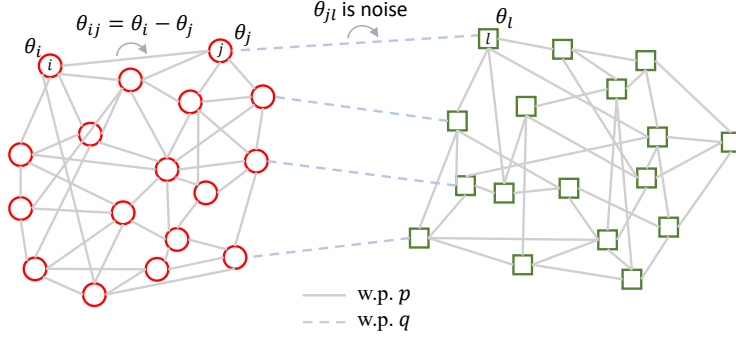


Figure 1: Illustration of the joint estimation problem on the network with two communities of equal size. Each node is associated with a phase. Each pair of nodes within the same community (resp. across communities) are independently connected with probability  $p$  (resp.  $q$ ) as shown in solid (resp. dash) lines. Also, a phase transition  $\theta_{ij} = \theta_i - \theta_j$  (resp.  $\theta_{ij}$  is noise) is observed on each edge  $(i, j)$  within each community (resp. across communities).

Under the random corruption model (Singer, 2011; Chen and Goldsmith, 2014), the observations constitute a Hermitian matrix whose  $(i, j)$ th entry for any  $i < j$  satisfies,

$$\mathbf{A}_{\text{Ph},ij} = \begin{cases} e^{\iota(\theta_i - \theta_j)}, & \text{with probability } r \in [0, 1], \\ u_{ij} \sim \text{Unif}(U(1)), & \text{with probability } 1 - r, \end{cases}$$

where  $\iota = \sqrt{-1}$  is the imaginary unit, and  $U(1)$  is unitary group of dimension 1. The most common formulation of the phase synchronization problem is through the following nonconvex optimization program

$$\max_{\mathbf{x} \in \mathbb{C}_1^N} \langle \mathbf{A}_{\text{Ph}}, \mathbf{x} \mathbf{x}^H \rangle, \quad (2)$$

where  $\mathbb{C}_1^N$  is the Cartesian product of  $N$  copies of  $U(1)$ . Again, similar to SBM, solving (2) is non-convex and NP-hard (Zhang and Huang, 2006). Many algorithms have been proposed for practical and approximate solutions of (2), including spectral and SDP relaxations (Singer, 2011; Cucuringu et al., 2012; Chaudhury et al., 2015; Bandeira et al., 2016, 2017), generalized power method (GPM) (Boumal, 2016; Liu et al., 2017; Zhong and Boumal, 2018). Besides, Bandeira et al. (2020); Perry et al. (2018); Gao and Zhao (2019) consider the phase synchronization problem in multiple frequency channels, which in general outperforms the formulation (2).

Recently, an increasing interest (Fan et al., 2021a,b; Chen et al., 2021) has been seen in the *joint community detection and phase (group) synchronization problem* (joint estimation problem, for brevity). As illustrated in Figure 1, the joint estimation problem assumes the data points associated with phase angles (or group elements) in a network fall into  $M$  underlying communities, and aims to simultaneously recover community memberships and associated phase angles (or group elements). The joint estimation problem is motivated by the 2D class averaging procedure in *cryo-electron microscopy single particle reconstruction* (Frank, 2006; Singer et al., 2011; Zhao and Singer, 2014), which aims to cluster 2D projection images taken from similar viewing directions, align ( $U(1)$  or  $SO(2)$  synchronization due to the in-plane rotation) and average projection images in each cluster to improve their signal-to-noise ratio.

In this paper, we study the joint estimation problem based on the probabilistic model, *stochastic block model with relative phase* (SBM-Ph), which is similar to the probabilistic model considered in (Fan et al., 2021a,b; Chen et al., 2021). Specifically, given  $N$  nodes in a network assigned into  $M$  underlying communities of equal size  $s = N/M$ , we assume that each node  $i$  is associated with an unknown phase  $\theta_i^* \in \Omega$ , where  $\Omega$  is a discretization of  $[0, 2\pi]^1$ . For each pair of nodes  $(i, j)$ , if they belong to the same community, their phase transition  $\theta_{ij} := (\theta_i - \theta_j) \bmod 2\pi$  can be obtained with probability  $p$ ; otherwise, we obtain noise generated uniformly at random from  $\Omega$  with probability  $q$ . The goal of the joint estimation problem is to simultaneously recover community memberships and associated phase angles. This problem can be formulated as an optimization program maximizing not only the

<sup>1</sup>We also extend the joint estimation problem into  $[0, 2\pi]$  in Section 3.3.

edge connections inside each community, but also the consistency among the observed phase transitions within each community. Still, such kind of optimization programs, similar to community detection on SBM (1) and phase synchronization (2), is non-convex. In Fan et al. (2021a), an SDP method is proposed to achieve approximate solutions with polynomial computational complexity. Fan et al. (2021b) then proposes a spectral method based on the block-wise column-pivoted QR (CPQR) factorization, which scales linearly with the number of edges in the network. The most recent work (Chen et al., 2021) develops an iterative GPM, where each iteration follows a matrix-multiplication-then-projection manner. The iterative GPM requires initialization, and the computational complexity of each iteration also scales linearly with the number of edges in the network<sup>2</sup>. However, existing methods are not developed from the MLE perspective, which limit their performance on the joint estimation problem.

## 1.1 Contributions

Unlike existing methods, this paper study the joint estimation problem by first studying its corresponding MLE formulation, which exhibits a “*multi-frequency*” structure (detailed in Section 3). More specifically, the MLE formulation is maximizing the summation over multiple frequency components, whose first frequency component is actually the objective function studied in Fan et al. (2021a,b); Chen et al. (2021). Based on the new insight, *a spectral method based on the multi-frequency column-pivoted QR (MF-CPQR) factorization and an iterative multi-frequency generalized power method (MF-GPM)* are proposed to tackle the MLE formulation of the joint estimation problem, and both achieve much higher accuracy in numerical experiments. The contributions of this paper can be summarized as follows:

- We study the MLE formulation of the joint community detection and phase synchronization problem with discretized phase angles, and show it contains a “*multi-frequency*” structure. In a similar manner, we introduce the truncated MLE for the joint estimation problem with continuous phase angles in  $[0, 2\pi]$ .
- Inspired by Fan et al. (2021b) and the “*multi-frequency*” nature of the MLE formulation, we propose a spectral method based on the novel MF-CPQR factorization. The MF-CPQR factorization is adjusted from the CPQR factorization to cope with information across multiple frequencies. Similarly, we also introduce an iterative MF-GPM by carefully designing steps of leveraging the “*multi-frequency*” structure.
- We compare the performance of our proposed methods to existing methods (Fan et al., 2021b; Chen et al., 2021) on both discrete and continuous phase angles in  $[0, 2\pi]$  via a series of numerical experiments. Our proposed methods achieve higher accuracy in estimating both community memberships and associated phase angles.

## 1.2 Organization

The rest of this paper is organized as follows. The formal definition of SBM-Ph, the MLE formulation of the joint estimation problem, and the extension to continuous phase angles, are detailed in Section 3. Section 4 and 5 present the spectral method based on the MF-CPQR factorization and the iterative MF-GPM, respectively. Numerical experiments are in Section 6. Finally, we conclude the paper in Section 7.

## 1.3 Notations

Throughout this paper, we use  $[n]$  to denote the set  $\{1, 2, \dots, n\}$ , and  $\mathbb{I}\{\cdot\}$  to denote the indicator function. The uppercase and lowercase letters in boldface are used to represent matrices and vectors, while normal letters are reserved for scalars.  $\|\mathbf{X}\|_{\text{F}}$  and  $\text{Tr}(\mathbf{X})$  denote the Frobenius norm and the trace of matrix  $\mathbf{X}$ , and  $\|\mathbf{v}\|_2$  denotes the  $\ell_2$  norm of the vector  $\mathbf{v}$ . The transpose and Hermitian transpose of a matrix  $\mathbf{X}$  (resp. a vector  $\mathbf{x}$ ) are denoted by  $\mathbf{X}^{\top}$  and  $\mathbf{X}^{\text{H}}$  (resp.  $\mathbf{x}^{\top}$  and  $\mathbf{x}^{\text{H}}$ ), respectively. An  $m \times n$  matrix of all zeros is denoted by  $\mathbf{0}_{m \times n}$  (or  $\mathbf{0}$ , for brevity). An identity matrix of size  $n \times n$  is defined as  $\mathbf{I}_n$ . The complex conjugate of  $x$  is denoted by  $\bar{x}$ . The inner product  $\langle \cdot, \cdot \rangle$  between two scalars, vectors, and matrices are  $\langle x, y \rangle = \bar{x}y$ ,  $\langle \mathbf{x}, \mathbf{y} \rangle = \mathbf{x}^{\text{H}}\mathbf{y}$ , and  $\langle \mathbf{X}, \mathbf{Y} \rangle = \text{Tr}(\mathbf{X}^{\text{H}}\mathbf{Y})$ , respectively.

---

<sup>2</sup>The bottleneck of each iteration is the matrix multiplication, which is  $\mathcal{O}(\# \text{ of edges})$  in general. To achieve  $\mathcal{O}(N \log^2 N)$  complexity claimed in Chen et al. (2021), one need to assume the graph is sparse.

In terms of indexing,  $(i, j)$ th entry of  $\mathbf{X}$  is denoted by  $\mathbf{X}_{ij}$ , and  $i$ th entry of  $\mathbf{x}$  is denoted by  $\mathbf{x}_i$ .  $\mathbf{X}_{i,\cdot}$  (resp.  $\mathbf{X}_{\cdot,j}$ ) is used to denote  $i$ th row (resp.  $j$ th column) of  $\mathbf{X}$ . We use  $\mathbf{X}_{i,j:}$  (resp.  $\mathbf{X}_{i:,j}$ ) to denote the segment of the  $i$ th row (resp.  $j$ th column) from the  $j$ th entry (resp.  $i$ th entry) to the end, and  $\mathbf{x}_{i:}$  to denote the segment from  $i$ th entry to the end. In addition, the sub-matrix of  $\mathbf{X}$  from the  $i$ th row and  $j$ th column to the end is denoted by  $\mathbf{X}_{i:,j:}$ .

For two non-negative functions  $f(n)$  and  $g(n)$ ,  $f(n) = \mathcal{O}(g(n))$  means there exists an absolute positive constant  $C$  such that  $f(n) \leq Cg(n)$  for all sufficiently large  $n$ ;  $f(n) = \Theta(g(n))$  if i)  $f(n) = \mathcal{O}(g(n))$ , and ii) there exists some positive constant  $C$  such that  $f(n) \geq C(g(n))$  for all sufficient large  $n$ ; and  $f(n) = o(g(n))$  indicates for every positive constant  $C$ , the inequality  $f(n) \leq Cg(n)$  holds for all sufficiently large  $n$ .

## 2 Preliminaries

In this section, we introduce some important definitions that will be used for our algorithms later.

**Definition 1** (Polar factorization). *For a matrix  $\mathbf{X} \in \mathbb{C}^{n \times n}$ , the polar factorization of  $\mathbf{X}$  is the factorization*

$$\mathbf{X} = \mathcal{P}(\mathbf{X})\mathbf{Z}$$

where  $\mathcal{P}(\mathbf{X}) \in \mathbb{C}^{n \times n}$  is unitary and  $\mathbf{Z} \in \mathbb{C}^{n \times n}$  is positive semi-definite.

Such a factorization always exists and, if  $\mathbf{X}$  has full rank,  $\mathbf{Z}$  is guaranteed to be positive definite. Importantly, in any unitarily-invariant norm,  $\mathcal{P}(\mathbf{X})$  is the closest unitary matrix to  $\mathbf{X}$ , i.e.,  $\mathcal{P}(\mathbf{X}) = \operatorname{argmin}_{\mathbf{Y} \in U(d)} \|\mathbf{X} - \mathbf{Y}\|_{\text{F}}$  (Fan and Hoffman, 1955). Let  $\mathbf{X} = \mathbf{U}\Sigma\mathbf{V}^H$  be its singular value decomposition, the corresponding polar factor can be easily computed as  $\mathcal{P}(\mathbf{X}) = \mathbf{U}\mathbf{V}^H$ .

**Definition 2** (QR factorization). *Given  $\mathbf{X} \in \mathbb{C}^{m \times n}$ , a QR factorization of  $\mathbf{X}$  satisfies*

$$\mathbf{X} = \mathbf{Q}\mathbf{R},$$

where  $\mathbf{Q} \in \mathbb{C}^{m \times m}$  is a unitary matrix, and  $\mathbf{R} \in \mathbb{C}^{m \times n}$  is an upper triangular matrix.

Such factorization always exists for any  $\mathbf{X}$ . The most common methods for computing the QR factorization are Gram-Schmidt process (Trefethen and Bau III, 1997), and Householder transformation (Bulirsch et al., 1991).

**Definition 3** (Column-pivoted QR factorization). *Let  $\mathbf{X} \in \mathbb{C}^{m \times n}$  with  $m \leq n$  has rank  $m$ . The column-pivoted QR factorization of  $\mathbf{X}$  is the factorization*

$$\mathbf{X}\boldsymbol{\Pi}_n = \mathbf{Q}[\mathbf{R}_1, \mathbf{R}_2],$$

as computed via the Golub-Businger algorithm (Businger and Golub, 1971) where  $\boldsymbol{\Pi}_n \in \{0, 1\}^{n \times n}$  is a permutation matrix,  $\mathbf{Q}$  is a unitary matrix,  $\mathbf{R}_1$  is an upper triangular matrix, and  $\mathbf{R}_2 \in \mathbb{C}^{m \times (n-m)}$ .

The ordinary QR factorization is proceeded on  $\mathbf{X}$  from the first column to the last column in order, whereas the order of the CPQR factorization is indicated by  $\boldsymbol{\Pi}_n$ . We refer to Businger and Golub (1971) for more details on the CPQR factorization.

**Definition 4** (Projection onto  $\mathcal{H}$  in (1)). *For arbitrary matrix  $\mathbf{X} \in \mathbb{R}^{m \times n}$ , we define*

$$\mathcal{P}_{\mathcal{H}}(\mathbf{X}) := \operatorname{argmin}_{\mathbf{H} \in \mathcal{H}} \|\mathbf{H} - \mathbf{X}\|_{\text{F}} = \operatorname{argmax}_{\mathbf{H} \in \mathcal{H}} \langle \mathbf{H}, \mathbf{X} \rangle$$

as the projection of  $\mathbf{X}$  onto  $\mathcal{H}$ .

The projection aims to find a set of community assignments that has the largest overall scores given by  $\mathbf{X}$ . Wang et al. (2021) finds that projection onto  $\mathcal{H}$  is equivalent to a *minimum-cost assignment problem* (MCAP), and can be efficiently solved (Tokuyama and Nakano, 1995) within  $\mathcal{O}(n^2m \log m)$  computational complexity.

### 3 Problem Formulation

In this section, we formally define the probabilistic model, *stochastic block model with relative phase*, studied in this paper. We first consider discrete phase angles and formulate the corresponding maximum likelihood estimation (MLE) problem, which exhibits a *multi-frequency* structure, to jointly recover the cluster structure and discrete phase angles. Then, we extend the problem to continuous phase angles and formulate a truncated MLE.

#### 3.1 Stochastic Block Model with Discrete Relative Phase Angles

Stochastic block model with relative phase (SBM-Ph) is considered in a network with  $N$  nodes and  $M \geq 2$  underlying communities of equal size  $s = N/M$ . We assume each node  $i \in [N]$  falls in one of the  $M$  underlying communities with the community membership  $\mathcal{M}^*(i) \in [M]$ , and is associated with an unknown phase angle  $\theta_i^* \in \Omega$ , where  $\Omega := \{0, \dots, (2K_{\max} + 1)\Delta\}$  is a discretization of  $[0, 2\pi)$  with  $\Delta = 2\pi/(2K_{\max} + 1)$ . We use  $\mathcal{S}_m^*$  to denote the set of nodes belonging to the  $m$ th community for all  $m \in [M]$ .

SBM-Ph generates a random graph  $\mathcal{G} = ([N], \mathcal{E})$  with the node set  $[N]$  and the edge set  $\mathcal{E} \subseteq [n] \times [n]$ . Each pair of nodes  $(i, j)$  are connected independently with probability  $p$  if  $i$  and  $j$  belong to the same community, or equivalently,  $\mathcal{M}^*(i) = \mathcal{M}^*(j)$ . Otherwise,  $i$  and  $j$  are connected independently with probability  $q$  if  $\mathcal{M}^*(i) \neq \mathcal{M}^*(j)$ . Meanwhile, a relative phase angle  $\theta_{ij} \in \Omega$  is observed on each edge  $(i, j) \in \mathcal{E}$ . When  $\mathcal{M}^*(i) = \mathcal{M}^*(j)$ , we obtain  $\theta_{ij} := (\theta_i^* - \theta_j^*) \bmod 2\pi$ . Otherwise, we observe  $\theta_{ij} := u_{ij} \sim \text{Unif}(\Omega)$ , which is drawn uniformly at random from  $\Omega$ .

Our observation model can be represented by the *observation matrix*  $\mathbf{A} \in \mathbb{C}^{N \times N}$ , which is a Hermitian matrix whose  $(i, j)$ th entry for any  $i < j$  satisfies,

$$\mathbf{A}_{ij} = \begin{cases} e^{\iota(\theta_i^* - \theta_j^*)}, & \text{with probability } p \text{ if } \mathcal{M}^*(i) = \mathcal{M}^*(j), \\ e^{\iota u_{ij}} : u_{ij} \sim \text{Unif}(\Omega), & \text{with probability } q \text{ if } \mathcal{M}^*(i) \neq \mathcal{M}^*(j), \\ 0, & \text{otherwise,} \end{cases} \quad (3)$$

where  $\mathbf{A}_{ji} = \overline{\mathbf{A}_{ij}}$  due to Hermitian. We also set the diagonal  $\mathbf{A}_{ii} = 0, \forall i \in [N]$ . Notice that a realization generated by the above observation matrix (3) is a noisy version of the *clean observation matrix*  $\mathbf{A}^{\text{clean}} \in \mathbb{C}^{N \times N}$ , whose  $(i, j)$ th entry satisfies,

$$\mathbf{A}_{ij}^{\text{clean}} = \begin{cases} e^{\iota(\theta_i^* - \theta_j^*)}, & \text{if } \mathcal{M}^*(i) = \mathcal{M}^*(j), \\ 0, & \text{otherwise.} \end{cases} \quad (4)$$

Specially,  $\mathbf{A}$  is equal to  $\mathbf{A}^{\text{clean}}$  when  $p = 1$  and  $q = 0$ .

**Remark 1.** Unlike the observation matrix (or adjacency matrix)  $\mathbf{A}_{\text{SBM}}$  in SBM (Abbe and Sandon, 2015; Abbe et al., 2015; Abbe, 2017; Bandeira, 2018) with only  $\{0, 1\}$ -valued entries,  $\mathbf{A}$  in (3) extends to incorporating the relative phase angles  $\theta_{ij}$  into edges. On the other hand, while entries of the observation matrix  $\mathbf{A}_{\text{Ph}}$  in the phase synchronization problem (Singer, 2011; Perry et al., 2018; Gao and Zhao, 2019) encode the pairwise transformation information, they do not have the underlying  $M$ -community structure.

#### 3.2 MLE with Multi-Frequency Nature

Based on the observation matrix  $\mathbf{A}$ , we detail the MLE for recovering the cluster membership and phase angles in this section. Given the parameters, the angles associated with nodes  $\{\theta_i \in \Omega\}_{i=1}^N$  and community assignments  $\{\mathcal{S}_m\}_{m=1}^M$  of equal size  $s$ , the probability model of observing  $\mathbf{A}_{ij}$  between node pair  $(i, j)$  is

$$\mathbb{P}(\mathbf{A}_{ij} | \{\theta_i \in \Omega\}_{i=1}^N, \{\mathcal{S}_m\}_{m=1}^M) = \begin{cases} p, & \text{if } \mathbf{A}_{ij} = e^{\iota(\theta_i - \theta_j)} \text{ and } \mathcal{M}(i) = \mathcal{M}(j), \\ 1 - p, & \text{if } \mathbf{A}_{ij} = 0 \text{ and } \mathcal{M}(i) = \mathcal{M}(j), \\ \frac{q}{K}, & \text{if } \mathbf{A}_{ij} = e^{\iota u_{ij}} : u_{ij} \in \Omega \text{ and } \mathcal{M}(i) \neq \mathcal{M}(j), \\ 1 - q, & \text{if } \mathbf{A}_{ij} = 0 \text{ and } \mathcal{M}(i) \neq \mathcal{M}(j), \end{cases}$$

where  $\mathcal{M}(\cdot)$  is the membership function corresponding to community assignments  $\{\mathcal{S}_m\}_{m=1}^M$ , and  $K = 2K_{\max} + 1$ . The likelihood function given the observations on the edge set  $\mathcal{E}$  is

$$\mathbb{P}(\{\mathbf{A}_{ij}\}_{(i,j) \in \mathcal{E}} \mid \{\theta_i \in \Omega\}_{i=1}^N, \{\mathcal{S}_m\}_{m=1}^M) = \prod_{\mathcal{M}(i)=\mathcal{M}(j), (i,j) \in \mathcal{E}} p^{\mathbb{I}\{\mathbf{A}_{ij}=e^{\iota(\theta_i-\theta_j)}\}} \prod_{\mathcal{M}(i) \neq \mathcal{M}(j), (i,j) \in \mathcal{E}} q/K, \quad (5)$$

due to the independence among edges within  $\mathcal{E}$ . Notice that maximizing the likelihood function (5) is equal to maximizing the following log-likelihood function

$$\begin{aligned} \log \mathbb{P}(\{\mathbf{A}_{ij}\}_{(i,j) \in \mathcal{E}} \mid \{\theta_i \in \Omega\}_{i=1}^N, \{\mathcal{S}_m\}_{m=1}^M) &= \sum_{\mathcal{M}(i)=\mathcal{M}(j), (i,j) \in \mathcal{E}} \mathbb{I}\{\mathbf{A}_{ij}=e^{\iota(\theta_i-\theta_j)}\} \log p \\ &+ \sum_{\mathcal{M}(i) \neq \mathcal{M}(j), (i,j) \in \mathcal{E}} \log q/K. \end{aligned} \quad (6)$$

Given  $0 < q/K < p$ , maximizing (6) is equivalent to

$$\max_{\{\theta_i \in \Omega\}_{i=1}^N, \{\mathcal{S}_m\}_{m=1}^M} \sum_{\mathcal{M}(i)=\mathcal{M}(j), (i,j) \in \mathcal{E}} \mathbb{I}\{\theta_{ij} = [(\theta_i - \theta_j) \bmod 2\pi]\}. \quad (7)$$

By taking the FFT w.r.t. the support  $\Omega$  of  $((\theta_i - \theta_j) \bmod 2\pi)$ s and inverse FFT (IFFT) back, (7) is equivalent to

$$\max_{\{\theta_i \in \Omega\}_{i=1}^N, \{\mathcal{S}_m\}_{m=1}^M} \sum_{k=-K_{\max}}^{K_{\max}} \sum_{m=1}^M \sum_{i,j \in \mathcal{S}_m} \langle \mathbf{A}_{ij}^{(k)}, e^{\iota k(\theta_i-\theta_j)} \rangle, \quad (8)$$

where  $\mathbf{A}^{(k)}$  is the  $k$ th entry-wise power of  $\mathbf{A}$  with  $\mathbf{A}_{ij}^{(k)} = e^{\iota k \theta_{ij}}$ .

As indicated by (8), the MLE exhibits a nature of *multi-frequency*, where the  $k$ th frequency component is  $\sum_{m=1}^M \sum_{i,j \in \mathcal{S}_m} \langle \mathbf{A}_{ij}^{(1)}, e^{\iota(\theta_i-\theta_j)} \rangle$  in (8). Although the following program using the first frequency component

$$\max_{\{\theta_i \in \Omega\}_{i=1}^N, \{\mathcal{S}_m\}_{m=1}^M} \sum_{m=1}^M \sum_{i,j \in \mathcal{S}_m} \langle \mathbf{A}_{ij}^{(1)}, e^{\iota(\theta_i-\theta_j)} \rangle, \quad (9)$$

is a reasonable formulation for the joint estimation problem as suggested by Fan et al. (2021a,b); Chen et al. (2021), it is indeed not a MLE formulation. One can show that (9) is equivalent to

$$\max_{\{\theta_i \in \Omega\}_{i=1}^N, \{\mathcal{S}_m\}_{m=1}^M} \sum_{\mathcal{M}(i)=\mathcal{M}(j), (i,j) \in \mathcal{E}} \cos(\theta_{ij} - (\theta_i - \theta_j)),$$

which is not the MLE (7) of the joint estimation problem.

To proceed, we perform a change of optimization variables for (8). By defining a unitary matrix  $\mathbf{V} \in \mathbb{C}^{N \times M}$  whose  $(i, m)$ th entry satisfies

$$V_{im} := \begin{cases} \frac{1}{\sqrt{s}} e^{\iota \theta_i}, & \text{if } i \in \mathcal{S}_m \text{ (or } \mathcal{M}(i) = m\text{),} \\ 0, & \text{otherwise,} \end{cases} \quad (10)$$

the community assignments  $\{\mathcal{S}_m\}_{m=1}^M$  and the associated phase angles  $\{\theta_i \in \Omega\}_{i=1}^N$  are encoded into one simple unitary matrix  $\mathbf{V}$ . Then, the optimization program (8) can be reformulated as

$$\begin{aligned} \max_{\mathbf{V} \in \mathbb{C}^{N \times M}} \quad & \sum_{k=-K_{\max}}^{K_{\max}} \left\langle \mathbf{A}^{(k)}, \mathbf{V}^{(k)} \left( \mathbf{V}^{(k)} \right)^H \right\rangle \\ \text{s.t.} \quad & \mathbf{V} \text{ satisfies the form (10),} \end{aligned} \quad (11)$$

where each  $\mathbf{V}^{(k)}$  is generated by  $\mathbf{V}$  through the entry-wise power that satisfies

$$V_{im}^{(k)} := \begin{cases} \frac{1}{\sqrt{s}} e^{\iota k \theta_i}, & \text{if } i \in \mathcal{S}_m \text{ (or } \mathcal{M}(i) = m\text{),} \\ 0, & \text{otherwise.} \end{cases} \quad (12)$$

The optimization program (11) is non-convex, and is thus computationally intractable to be solved exactly. Although one can try SDP based approaches similar to Fan et al. (2021a), it is not guaranteed to obtain exact solutions to the MLE, let alone the high computational complexity when  $N$  and  $K_{\max}$  are large. Therefore, we propose a spectral method based on the MF-CPQR factorization and the iterative MF-GPM in Section 4 and Section 5, respectively.

### 3.3 Extension to Continuous Phase Angles: Truncated MLE

We consider the joint estimation problem on a discretization of  $[0, 2\pi)$  in Section 3.1 and then derive the MLE formulation in Section 3.2. Now, we turn to the joint estimation problem with continuous phase angles in  $[0, 2\pi)$  ( $\theta_i \in [0, 2\pi), \forall i \in [N]$ ).

Following the similar steps as (5), (6), (7), the MLE formulation is

$$\max_{\{\theta_i \in [0, 2\pi)\}_{i=1}^N, \{\mathcal{S}_m\}_{m=1}^M} \sum_{\mathcal{M}(i)=\mathcal{M}(j), (i, j) \in \mathcal{E}} \mathbb{I}([( \theta_i - \theta_j) \bmod 2\pi] = \theta_{ij}). \quad (13)$$

The MLE formulation (13) is essentially equal to counting the times that  $\delta([( \theta_i - \theta_j) \bmod 2\pi] = \theta_{ij}) = \infty$ , where  $\delta(\cdot)$  is the Dirac delta function. We can express the Dirac delta function with its Fourier series expansion,

$$\delta([( \theta_i - \theta_j) \bmod 2\pi] = \theta_{ij}) = \sum_{k=-\infty}^{+\infty} e^{\iota k(\theta_i - \theta_j)} e^{-\iota k\theta_{ij}} \approx \sum_{k=-K_{\max}}^{K_{\max}} e^{\iota k(\theta_i - \theta_j)} e^{-\iota k\theta_{ij}}. \quad (14)$$

The straightforward truncation in (14) corresponds to approximating the Dirac delta with the *Dirichlet kernel*. By this truncation, the problem in (13) is converted to

$$\max_{\{\theta_i \in [0, 2\pi)\}_{i=1}^N, \{\mathcal{S}_m\}_{m=1}^M} \sum_{k=-K_{\max}}^{K_{\max}} \sum_{m=1}^M \sum_{i, j \in \mathcal{S}_m} \left\langle \mathbf{A}_{ij}^{(k)}, e^{\iota k(\theta_i - \theta_j)} \right\rangle. \quad (15)$$

The optimization program (15) is a truncated MLE of the joint estimation problem with continuous phase angles of (13).

As one can observe from (8) and (15), the only difference is that  $\theta_i \in \Omega$  is discrete in (8), and  $\theta_i \in [0, 2\pi)$  is continuous in (15). Algorithms in Section 4 and 5 can also be directly applied to the joint estimation problem with continuous phase angles after simple modification. Due to the similarity between the joint estimation problem and its continuous extension, we will only focus on the joint estimation problem on  $\Omega$  (despite numerical experiments) in the remaining parts of this paper for brevity.

## 4 Spectral Method Based on the MF-CPQR Factorization

In this section, we propose a spectral method based on the MF-CPQR factorization for the joint estimation problem. We start with introducing main steps and motivations of Algorithm 1 in Section 4.1. Section 4.2 states the novel algorithm, the MF-CPQR factorization, designed for our spectral method, together with the difference between the MF-CPQR factorization and the CPQR factorization. In Section 4.3, we discuss the computational complexity of our proposed algorithm in details.

Our spectral method based on MF-CPQR factorization is inspired by the CPQR-type algorithms (Damle et al., 2016; Fan et al., 2021b), together with the *multi-frequency* nature of the MLE formulation (11). Similar to the CPQR-type algorithms, Algorithm 1 is deterministic and free of any random initialization. Meanwhile, in terms of computational complexity, Algorithm 1 scales linearly w.r.t. the number of edges  $|\mathcal{E}|$  and near-linearly ( $K_{\max} \log K_{\max}$ ) w.r.t.  $K_{\max}$ .

### 4.1 Motivations

Algorithm 1 consists of three steps. It first computes the matrices  $\{\Phi^{(k)}\}_{k=-K_{\max}}^{K_{\max}}$  that contain the top  $M$  eigenvectors of each  $\mathbf{A}^{(k)}$  via eigendecomposition. Secondly, the matrices  $\{\mathbf{R}^{(k)}\}_{k=-K_{\max}}^{K_{\max}}$  are obtained through the MF-CPQR

---

**Algorithm 1:** The spectral method based on the MF-CPQR factorization

---

**Input:** The observation matrix  $\mathbf{A}$ , and the number of communities  $M$ .

1. (Eigendecomposition) For  $k = -K_{\max}, \dots, K_{\max}$ , compute top  $M$  eigenvectors  $\Phi^{(k)} \in \mathbb{C}^{N \times M}$  of  $\mathbf{A}^{(k)}$  such that  $(\Phi^{(k)})^H \Phi^{(k)} = \mathbf{I}_M$
2. (MF-CPQR factorization) Compute the multi-frequency column-pivoted QR factorization (detailed in Algorithm 2) of  $\left\{(\Phi^{(k)})^T\right\}_{k=-K_{\max}}^{K_{\max}}$ , which yields

$$(\Phi^{(k)})^T \Pi_N = \mathbf{Q}^{(k)} \mathbf{R}^{(k)} \Rightarrow (\Phi^{(k)})^T = \mathbf{Q}^{(k)} \mathbf{R}^{(k)} \Pi_N^T \quad (16)$$

Update  $\mathbf{R}^{(k)} \leftarrow \mathbf{R}^{(k)} \Pi_N^T, \forall k = -K_{\max}, \dots, K_{\max}$

3. (Recovery of community memberships and associated phase angles) For each node  $i \in [N]$ , assign its community membership as

$$\hat{\mathcal{M}}(i) \leftarrow \operatorname{argmax}_{m \in [M]} \left\{ \max_{\theta_i \in \Omega} \sum_{k=-K_{\max}}^{K_{\max}} \left\langle e^{\iota k \theta_i}, \mathbf{R}_{mi}^{(k)} \right\rangle \right\} \quad (17)$$

Then estimate the phase given the recovered community membership  $\hat{\mathcal{M}}(i)$

$$\hat{\theta}_i \leftarrow \operatorname{argmax}_{\theta_i \in \Omega} \sum_{k=-K_{\max}}^{K_{\max}} \left\langle e^{\iota k \theta_i}, \mathbf{R}_{\hat{\mathcal{M}}(i)i}^{(k)} \right\rangle \quad (18)$$

---

**Output:** Estimated community memberships  $\{\hat{\mathcal{M}}(i)\}_{i=1}^N$  and estimated phase angles  $\{\hat{\theta}_i\}_{i=1}^N$

---

factorization, which is detailed in Algorithm 2. The last step is recovering community memberships and associated phase angles based on  $\{\mathbf{R}^{(k)}\}_{k=-K_{\max}}^{K_{\max}}$  via (17) and (18).

In terms of motivations for Algorithm 1, we start from the MLE formulation (11). We first relax (11) by replacing the constraints in (10) with  $\mathbf{V}^H \mathbf{V} = \mathbf{I}_M$ ,

$$\Phi = \operatorname{argmax}_{\mathbf{V} \in \mathbb{C}^{N \times M}} \sum_{k=-K_{\max}}^{K_{\max}} \left\langle \mathbf{A}^{(k)}, \mathbf{V}^{(k)} (\mathbf{V}^{(k)})^H \right\rangle \quad \text{s.t. } \mathbf{V}^H \mathbf{V} = \mathbf{I}_M, \quad (19)$$

by noticing that  $\mathbf{V}$  in (10) forms an orthonormal basis. The optimization problem in (19) is still non-convex and there is no simple spectral method that can directly solve the problem. One approach is to relax the dependency of  $\mathbf{V}^{(k)}$  among different frequencies and split (19) into different frequencies, and that is, for  $k = -K_{\max}, \dots, K_{\max}$ , we determine

$$\Phi^{(k)} = \operatorname{argmax}_{\mathbf{V}^{(k)} \in \mathbb{C}^{N \times M}} \left\langle \mathbf{A}^{(k)}, \mathbf{V}^{(k)} (\mathbf{V}^{(k)})^H \right\rangle \quad \text{s.t. } (\mathbf{V}^{(k)})^H \mathbf{V}^{(k)} = \mathbf{I}_M. \quad (20)$$

It is straightforward to figure out the optimizer of (20) is the top  $M$  eigenvectors of  $\mathbf{A}^{(k)}$  denoted by  $\Phi^{(k)} \in \mathbb{C}^{N \times M}$ . This accounts for step 1 (eigendecomposition) in Algorithm 1.

In fact, we can get cluster membership from individual  $\Phi^{(k)}$ . To see this, for  $k = -K_{\max}, \dots, K_{\max}$ , we split  $\mathbf{A}^{(k)}$  into deterministic and random parts:

$$\mathbf{A}^{(k)} = \mathbb{E}[\mathbf{A}^{(k)}] + (\mathbf{A}^{(k)} - \mathbb{E}[\mathbf{A}^{(k)}]) = \mathbb{E}[\mathbf{A}^{(k)}] + \Delta^{(k)}, \quad (21)$$

where  $\mathbb{E}[\mathbf{A}^{(k)}] = p \mathbf{A}_{\text{clean}}^{(k)}$  with  $\mathbf{A}_{\text{clean}}^{(k)}$  being the entry-wise  $k$ th power of  $\mathbf{A}_{\text{clean}}$  (4), and the residual  $\Delta^{(k)}$  is a random perturbation with  $\mathbb{E}[\Delta^{(k)}] = \mathbf{0}$ . Obviously, each  $\mathbb{E}[\mathbf{A}^{(k)}]$  is a low rank matrix that satisfies the following

eigendecomposition:

$$\mathbb{E}[\mathbf{A}^{(k)}] = ps \sum_{m=1}^M \Psi_{\cdot,m}^{(k)} \left( \Psi_{\cdot,m}^{(k)} \right)^H, \quad \text{with} \quad \Psi_{im}^{(k)} := \begin{cases} \frac{1}{\sqrt{s}} e^{\iota k \theta_i^*}, & \text{if } i \in \mathcal{S}_m^*, \\ 0, & \text{otherwise,} \end{cases}$$

where  $\Psi^{(k)} \in \mathbb{C}^{N \times M}$  is a matrix defined in a similar manner as  $\mathbf{V}^{(k)}$  in (12), and satisfies  $(\Psi^{(k)})^H \Psi^{(k)} = \mathbf{I}_M$ . Then, for  $k = -K_{\max}, \dots, K_{\max}$  (except for  $k = 0$ ), the non-zero entry in each row of  $\Psi^{(k)}$  indicates the underlying community membership  $\mathcal{M}^*(i)$  and the exact phase  $\theta_i^*$  of node  $i$ .

To the ease of illustration, we first consider the case when  $p = 1$  and  $q = 0$ . This indicates, for  $k = -K_{\max}, \dots, K_{\max}$ ,  $\mathbf{A}^{(k)} = \mathbf{A}_{\text{clean}}^{(k)}$ ,  $\Delta^{(k)} = \mathbf{0}$ , and  $\Phi^{(k)} = \Psi^{(k)} \mathbf{O}^{(k)}$ , where  $\mathbf{O}^{(k)} \in \mathbb{C}^{M \times M}$  is some unitary matrix. For recovering community memberships and associated phase angles, it suffices to extract  $\{\Psi^{(k)}\}_{k=-K_{\max}}^{K_{\max}}$  from  $\{\Phi^{(k)}\}_{k=-K_{\max}}^{K_{\max}}$ . However, such extraction is non-trivial as  $\{\mathbf{O}^{(k)}\}_{k=-K_{\max}}^{K_{\max}}$  is unknown and even not consistent among all frequencies. Here, we assume that the first  $s$  nodes are from the community  $\mathcal{S}_1^*$ , the following  $s$  nodes are from  $\mathcal{S}_2^*$ , and so on. Applying the MF-CPQR factorization (step 2) in Algorithm 1 yields (assume  $\Pi_N = \mathbf{I}_N$ )

$$\begin{aligned} \left( \Phi^{(k)} \right)^T &= \left( \mathbf{O}^{(k)} \right)^T \left( \Psi^{(k)} \right)^T \\ &= \left( \mathbf{O}^{(k)} \right)^T \begin{bmatrix} \frac{1}{\sqrt{s}} e^{\iota k \theta_1^*} & \dots & \frac{1}{\sqrt{s}} e^{\iota k \theta_s^*} & \dots & 0 & \dots & 0 \\ \vdots & \vdots & \vdots & \ddots & \vdots & \vdots & \vdots \\ 0 & \dots & 0 & \dots & \frac{1}{\sqrt{s}} e^{\iota k \theta_{N-s+1}^*} & \dots & \frac{1}{\sqrt{s}} e^{\iota k \theta_N^*} \end{bmatrix} \\ &= \left( \mathbf{O}^{(k)} \right)^T \underbrace{\begin{bmatrix} e^{\iota k \theta_1^*} & \dots & 0 \\ \vdots & \ddots & \vdots \\ 0 & \dots & e^{\iota k \theta_{N-s+1}^*} \end{bmatrix}}_{=: \mathbf{Q}^{(k)}} \quad (22) \\ &\quad \times \underbrace{\begin{bmatrix} \frac{1}{\sqrt{s}} & \dots & \frac{1}{\sqrt{s}} e^{\iota k(\theta_s^* - \theta_1^*)} & \dots & 0 & \dots & 0 \\ \vdots & \vdots & \vdots & \ddots & \vdots & \vdots & \vdots \\ 0 & \dots & 0 & \dots & \frac{1}{\sqrt{s}} & \dots & \frac{1}{\sqrt{s}} e^{\iota k(\theta_N^* - \theta_{N-s+1}^*)} \end{bmatrix}}_{=: \mathbf{R}^{(k)}} \\ &= \mathbf{Q}^{(k)} \mathbf{R}^{(k)}, \end{aligned}$$

for  $k = -K_{\max}, \dots, K_{\max}$ . Therefore, each  $\mathbf{Q}^{(k)} \in \mathbb{C}^{M \times M}$  is a unitary matrix that includes the unknown unitary matrix  $\mathbf{O}^{(k)}$ , and each  $\mathbf{R}^{(k)} \in \mathbb{C}^{M \times N}$  is a matrix excludes  $\mathbf{O}^{(k)}$ . More significantly,  $\{\mathbf{R}^{(k)}\}_{k=-K_{\max}}^{K_{\max}}$  contains all the information needed for recovering the community memberships and the associated phase angles.

To recover the community memberships, the CPQR-type algorithm (Fan et al., 2021b) only uses  $\mathbf{R}^{(1)}$ . By noticing that for each node  $i$ , the  $i$ th column of  $\mathbf{R}^{(1)}$  (e.g.,  $\mathbf{R}_{\cdot,i}^{(1)}$ ) is sparse such that its  $m$ th entry  $\mathbf{R}_{mi}^{(1)}$  is nonzero only if  $m = \mathcal{M}^*(i)$ , one can determine the community membership of node  $i$  by the position of the nonzero entry. Meanwhile, the associated phase can also be determined by obtaining the phase from the nonzero entry (up to some global phase transition in the same community). When the observation  $\mathbf{A}$  is noisy, the CPQR-type algorithm recovers the community membership and associated phase of node  $i$  by the position of the entry with the largest amplitude. The following Theorem 1 proves as long as the perturbation to  $\mathbb{E}[\mathbf{A}^{(k)}]$  is less than a certain threshold,  $\Phi^{(k)}$  is still close to  $\Psi^{(k)} \mathbf{O}^{(k)}$ , for  $k = -K_{\max}, \dots, K_{\max}$  (except for  $k = 0$ ).

**Theorem 1** (Row-wise error bound, adapted from Fan et al. (2021b)). *Given a network with  $N$  nodes and  $M = 2$  underlying communities, for a sufficiently large  $N$ , we suppose*

$$\eta := \frac{\sqrt{(p(1-p) + q) \log N}}{p\sqrt{N}} \leq c_0$$

for some small constant  $c_0$ . Consequently, with probability at least  $1 - \mathcal{O}(N^{-1})$ ,

$$\max_{i \in [N]} \left\| \Phi_{i,\cdot}^{(k)} - \Psi_{i,\cdot}^{(k)} \mathbf{O}^{(k)} \right\|_2 \lesssim \frac{\eta}{\sqrt{N}},$$

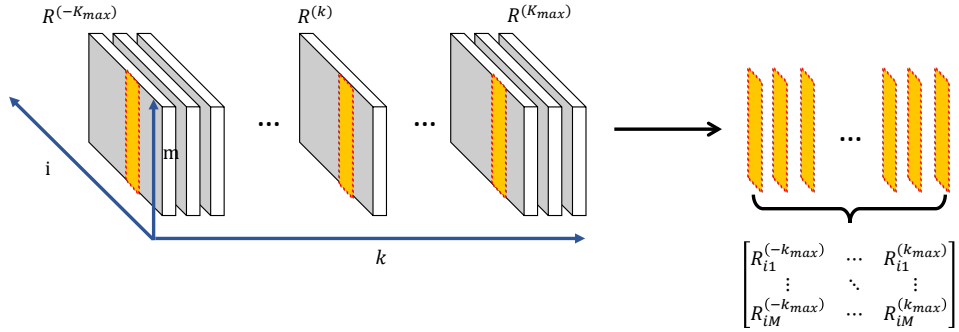


Figure 2: Illustration of step 3 in Algorithm 1. For  $i \in [N]$ , we take the  $i$ th columns across all frequencies to estimate the community membership and phase.

where  $\mathbf{O}^{(k)} = \mathcal{P}((\Psi^{(k)})^\mathsf{H} \Phi^{(k)})$ .

Theorem 1 guarantees i) the amplitude of other entries are less than the entry indicating the true community membership with high probability, ii) the phase information is preserved with high fidelity. By applying the CPQR-type algorithm to the joint estimation problem, one can have the following performance guarantee.

Theorem 1 can be proved by following the same routines in Fan et al. (2021b) by replacing the orthogonal group element  $O_i$  with the  $U(1)$  group element (e.g.,  $e^{i\theta_i}$ ). The reason why Theorem 1 holds for  $k = -K_{\max}, \dots, K_{\max}$  (despite  $k = 0$ ) is due to the statistics of random perturbations  $\{\Delta^{(k)}\}_k$  in (21) do not change over frequencies. This is because the noise models of  $A^{(k)}$  and  $A$  are the same. The noisy entry  $e^{i u_{ij}} : u_{ij} \sim \text{Unif}(\Omega)$  in (3) has the same statistics as  $e^{i k u_{ij}}$  in  $A^{(k)}$  due to the fact that  $k u_{ij}$  still yields the distribution  $\text{Unif}(\Omega)$ . One should notice that the CPQR-type algorithm in (Fan et al., 2021b) is not developed from the MLE formulation (11) of the joint estimation problem, and thus does not capture the *multi-frequency* nature.

In this paper, we leverage  $\{\mathbf{R}^{(k)}\}_{k=-K_{\max}}^{K_{\max}}$  that contain information about community memberships and associated phase angles across multiple frequencies (step 3). Specifically, we first consider the case as (22) for intuition. As illustrated in Figure 2, the matrix concatenated by the  $i$ th ( $i \leq s$ ) columns across all frequencies is

$$\begin{bmatrix} \mathbf{R}_{i1}^{(-K_{\max})} & \dots & \mathbf{R}_{i1}^{(k)} & \dots & \mathbf{R}_{i1}^{(K_{\max})} \\ \vdots & \vdots & \vdots & \ddots & \vdots \\ \mathbf{R}_{iM}^{(-K_{\max})} & \dots & \mathbf{R}_{iM}^{(k)} & \dots & \mathbf{R}_{iM}^{(K_{\max})} \end{bmatrix} = \begin{bmatrix} \frac{1}{\sqrt{s}} e^{-\iota K_{\max}(\theta_i^* - \theta_1^*)} & \dots & \frac{1}{\sqrt{s}} e^{\iota k(\theta_i^* - \theta_1^*)} & \dots & \frac{1}{\sqrt{s}} e^{\iota K_{\max}(\theta_i^* - \theta_1^*)} \\ \vdots & \vdots & \vdots & \vdots & \vdots \\ 0 & \dots & 0 & \dots & 0 \end{bmatrix}.$$

The community membership of  $i$  can be acquired by finding the non-sparse row of the above matrix, and the phase can be determined by evaluating the non-sparse row (e.g., fast Fourier transform (FFT)). When the observation  $A$  is noisy, (17) and (18) are used to estimate the community membership and phase, which can be interpreted as checking the consistency or majority vote among multiple frequencies. The performance is expected to be at least as good as the CPQR-type algorithm. This is because each  $\Phi^{(k)}$  has the same theoretical guarantee as the CPQR-type algorithm as shown in Theorem 1, and (17) (18) are just checking the consistency across all frequencies. In Section 6, we will show that our proposed spectral method based on the MF-CPQR factorization is capable of largely improving the performance over the CPQR-type algorithm.

Besides, for the joint estimation problem with continuous phase angles, (17) and (18) will be modified as

$$\hat{\mathcal{M}}(i) \leftarrow \operatorname{argmax}_{m \in [M]} \left\{ \max_{\theta_i \in [0, 2\pi)} \sum_{k=-K_{\max}}^{K_{\max}} \left\langle e^{\iota k \theta_i}, \mathbf{R}_{mi}^{(k)} \right\rangle \right\},$$

$$\hat{\theta}_i \leftarrow \operatorname{argmax}_{\theta_i \in [0, 2\pi)} \sum_{k=-K_{\max}}^{K_{\max}} \left\langle e^{\iota k \theta_i}, \mathbf{R}_{\hat{\mathcal{M}}(i)i}^{(k)} \right\rangle.$$

Solving the max problem over  $[0, 2\pi]$  is hard in general. Instead, we can use the zero-padding and FFT for an approximate solution with the desired precision. Specifically, in estimating the community membership, by padding

---

**Algorithm 2:** MF-CPQR factorization

---

**Input:** The set of eigenvectors  $\{\Phi^{(k)}\}_{k=-K_{\max}}^{K_{\max}}$

**Init:**  $\mathbf{Q}^{(k)} \leftarrow \mathbf{I}_M$ ,  $\mathbf{R}^{(k)} \leftarrow (\Phi^{(k)})^\top$ ,  $\forall i = -K_{\max}, \dots, K_{\max}$ , and  $\mathbf{\Pi}_N \leftarrow \mathbf{I}_N$

1 **for**  $m = 1, 2, \dots, M$  **do**

2     /\* Pivot selection \*/

3     **for**  $j = m, m+1, \dots, N$  **do**

4         Compute the residual  $\rho_j \leftarrow \sum_{k=-K_{\max}}^{K_{\max}} \|\mathbf{R}_{m:,j}^{(k)}\|_2$

5     **end**

6     Determine the pivot  $j^* \leftarrow \operatorname{argmax}_{j=m, \dots, N} \rho_j$

7     For both  $\{\mathbf{R}^{(k)}\}_{k=1}^{K-1}$  and  $\mathbf{\Pi}_N$ , swap the  $m$ th column with the pivot ( $j^*$ th) column

8     /\* One step QR factorization for all frequencies \*/

9     **for**  $k = -K_{\max}, \dots, K_{\max}$  **do**

10         Apply one step QR factorization in Algorithm 3 on  $\mathbf{R}_{m:,m}^{(k)}$ , and get  $\tilde{\mathbf{Q}}_{m:,m}^{(k)}$  and  $\tilde{\mathbf{R}}_{m:,m}^{(k)}$

11         Update  $\mathbf{Q}_m^{(k)} \leftarrow \begin{bmatrix} \mathbf{I}_{m-1} & \mathbf{0} \\ \mathbf{0} & \tilde{\mathbf{Q}}_{m:,m}^{(k)} \end{bmatrix}$

12         Update  $\mathbf{R}_{m:,m}^{(k)} \leftarrow \tilde{\mathbf{R}}_{m:,m}^{(k)}$  and  $\mathbf{Q}^{(k)} \leftarrow \mathbf{Q}^{(k)} \mathbf{Q}_m^{(k)}$

13     **end**

14 **end**

**Output:**  $\{\mathbf{Q}^{(k)}\}_{k=-K_{\max}}^{K_{\max}}$ ,  $\{\mathbf{R}^{(k)}\}_{k=-K_{\max}}^{K_{\max}}$ , and  $\mathbf{\Pi}_N$

---



---

**Algorithm 3:** One step QR factorization using Householder transformation

---

**Input:** A matrix  $\mathbf{X} \in \mathbb{C}^{n \times n}$

/\* Householder transformation \*/

1  $\mathbf{r} \leftarrow \mathbf{X}_{\cdot,1}$

2  $\theta \leftarrow -e^{i\angle \mathbf{r}_1} \|\mathbf{r}\|$ , where  $\angle \mathbf{r}_1$  is the phase of  $\mathbf{r}_1$

3  $\mathbf{u} \leftarrow \mathbf{r} - \theta \mathbf{e}$ , where  $\mathbf{e} = [1, 0, \dots, 0]^\top$

4  $\mathbf{v} \leftarrow \frac{\mathbf{u}}{\|\mathbf{u}\|}$

5  $\mathbf{Q} \leftarrow \mathbf{I}_n - 2\mathbf{v}\mathbf{v}^\mathsf{H}$

6  $\mathbf{X} \leftarrow \mathbf{Q}\mathbf{X}$

7  $\mathbf{X}_{1,\cdot} \leftarrow e^{-i\angle \mathbf{X}_{11}} \mathbf{X}_{1,\cdot}$

8  $\mathbf{Q}_{\cdot,1} \leftarrow e^{i\angle \mathbf{X}_{11}} \mathbf{Q}_{\cdot,1}$

**Output:**  $\mathbf{Q}$  and  $\mathbf{R}$

---

zeros to  $[\mathbf{R}_{mi}^{(-K_{\max})}, \dots, \mathbf{R}_{mi}^{(k)}, \dots, \mathbf{R}_{mi}^{(K_{\max})}]$  as  $[0, \dots, 0, \mathbf{R}_{mi}^{(-K_{\max})}, \dots, \mathbf{R}_{mi}^{(k)}, \dots, \mathbf{R}_{mi}^{(K_{\max})}, 0, \dots, 0]$ , taking the FFT, and finding the entry with largest real part, we can approximately solve  $(\arg) \max_{\theta_i \in [0, 2\pi)} \sum_{k=-K_{\max}}^{K_{\max}} \langle e^{ik\theta_i}, \mathbf{R}_{mi}^{(k)} \rangle$ , where the precision is determined by the number of padded zeros.

## 4.2 MF-CPQR Factorization

As stated in Definition 3, the difference between the ordinary QR factorization and the CPQR factorization is selecting appropriate pivot ordering (encoded in  $\mathbf{\Pi}_N$ ). The CPQR factorization attempts to find a subset of columns that are as most linearly independent as possible and are used to determine the basis. In this paper, the CPQR factorization across multiple frequencies is developed to cope with the *multi-frequency* structure of the MLE formulation.

**Definition 5** (Multi-frequency column-pivoted QR factorization). *Let  $\mathbf{X}^{(k)} \in \mathbb{C}^{m \times n}$  with  $m \leq n$  has rank  $m$  for  $k = -K_{\max}, \dots, K_{\max}$ . The multi-frequency column-pivoted QR factorization of  $\mathbf{X}^{(k)}$  is the factorization*

$$\mathbf{X}^{(k)} \mathbf{\Pi}_n = \mathbf{Q}^{(k)} \left[ \mathbf{R}_1^{(k)}, \mathbf{R}_2^{(k)} \right],$$

as computed via Algorithm 2 where  $\Pi_n \in \{0, 1\}^{n \times n}$  is a permutation matrix fixed for all  $k = -K_{\max}, \dots, K_{\max}$ ,  $Q^{(k)}$  is a unitary matrix,  $R_1^{(k)}$  is an upper triangular matrix, and  $R_2^{(k)} \in \mathbb{C}^{m \times (n-m)}$ .

It requires to i) obtain the same subset of columns among all frequencies that are as most linearly independent as possible, and ii) use the same pivot ordering (or  $\Pi_N$ ) among all frequencies. The former promotes the community assignments performance because the node  $i$  other than the pivots are assigned mainly by the similarity between the column  $i$  and the columns of pivots, the latter ensures the validity of (17) and (18).

The MF-CPQR factorization is detailed in Algorithm 2, where the Householder transform (Bulirsch et al., 1991) (Algorithm 3) is adopted for better numerical stability. Specifically, the novel MF-CPQR factorization is different from the ordinary CPQR (Golub and Van Loan, 1996; Trefethen and Bau III, 1997) in the pivot selection. The pivot is determined by finding the column with the largest summation of  $\ell_2$  norm of residuals over all frequencies (see line 3 in Algorithm 2).

### 4.3 Computational Complexity

In this section, the computational complexity of Algorithm 1 is summarized step by step in Table 1. Here, we suppose  $M = \Theta(1)$ . First, it consists of  $\mathcal{O}(K_{\max})$  times of eigendecomposition for  $M$  eigenvectors, which is  $\mathcal{O}(|\mathcal{E}|)$  per time if using Lanczos method (Stewart, 2002). For the MF-CPQR factorization, it consists of  $M$  times of column pivoting ( $\mathcal{O}(NK_{\max})$  per time) and  $MK_{\max}$  times of one step QR factorization ( $\mathcal{O}(N)$  per step). In terms of recovering the community memberships, we first compute  $MN$  times of FFT for length- $K_{\max}$  vectors ( $\mathcal{O}(K_{\max} \log K_{\max})$  per vector) and then compute the maximums ( $\mathcal{O}(NK_{\max}) + \mathcal{O}(N)$ ). Since the FFT of  $\{\mathbf{R}^{(k)}\}_{k=-K_{\max}}^{K_{\max}}$  is already computed, it is only  $\mathcal{O}(N)$  for synchronizing the phase angles. Overall, the computational cost is linear with the number of edges  $|\mathcal{E}|$  and nearly linear in  $K_{\max}$ . When the network  $\mathcal{G}$  is densely connected with  $|\mathcal{E}| = \mathcal{O}(N^2)$ , Algorithm 1 ends up with  $\mathcal{O}(K_{\max}N^2)$  if  $\log K_{\max} < N$ . However, if  $|\mathcal{E}| = o(N^2)$ , the complexity of Algorithm 1 will be reduced. For instance, in the case when  $|\mathcal{E}| = \mathcal{O}(N \log N)$  or  $|\mathcal{E}| = \mathcal{O}(N)$ , which is very common as shown in Leskovec et al. (2008), the complexity of Algorithm 1 will be  $\mathcal{O}(K_{\max}N \max\{\log N, \log K_{\max}\})$  or  $\mathcal{O}(K_{\max}N \log K_{\max})$ , respectively.

## 5 Iterative Multi-Frequency Generalized Power Method

In addition to the spectral method based on the MF-CPQR factorization proposed in Section 4, we develop an iterative multi-frequency generalized power method for the joint estimation problem, which is inspired by the generalized power method (Chen et al., 2021) and the “*multi-frequency*” nature of the MLE formulation (11).

### 5.1 Detailed Steps and Motivations

The algorithm is detailed in Algorithm 4, which requires an initialization of community memberships and associated phases. The initialization should be close enough to the ground truth, and can be realized by spectral methods (e.g., CPQR-type algorithm (Fan et al., 2021b, Algorithm 1) or (Chen et al., 2021, Algorithm 3)), which is similar as pointed in Chen et al. (2021). It is observed in experiments that random initialization will result in non-convergence. Algorithm 4 is then proceeded into the iteration process, where each iteration consists of 3 major steps. The first step (line 3) is the matrix multiplication between  $\mathbf{A}^{(k)}$  and  $\widehat{\mathbf{V}}^{(k),t}$  for all  $k = -K_{\max}, \dots, K_{\max}$  (line 4). Then we leverage (line 4)  $\widehat{\mathbf{V}}^{(k),t+1}$  across multiple frequencies to aggregate and refine the information needed for the joint

Table 1: The computational complexity of Algorithm 1 in each step.

Steps	Computational Complexity
1. Eigendecomposition	$\mathcal{O}(K_{\max} \mathcal{E} )$
2. MF-CPQR factorization	$\mathcal{O}(K_{\max}N)$
3. Recovering community memberships by (17)	$\mathcal{O}(NK_{\max} \log K_{\max})$
4. Phase synchronization by (18)	$\mathcal{O}(N)$
Total complexity	$\mathcal{O}(K_{\max}( \mathcal{E}  + N \log K_{\max}))$

---

**Algorithm 4:** Iterative multi-frequency generalized power method

---

**Input:** The observation matrix  $\mathbf{A}$ , the initialization  $\{\mathcal{S}_m\}_{m=1}^M$  and  $\{\theta_i \in \Omega\}_{i=1}^N$ , and the number of iterations  $T$

1 Construct  $\{\widehat{\mathbf{V}}^{(k),0}\}_{k=-K_{\max}}^{K_{\max}}$  using  $\{\mathcal{S}_m\}_{m=1}^M$  and  $\{\theta_i \in \Omega\}_{i=1}^N$  according to (12)

2 **for**  $t = 0, 1, \dots, T-1$  **do**

/\* Matrix multiplication \*/

3 For  $k = -K_{\max}, \dots, K_{\max}$ , compute the matrix multiplication  $\widehat{\mathbf{V}}^{(k),t+1} \leftarrow \mathbf{A}^{(k)} \widehat{\mathbf{V}}^{(k),t}$

/\* Combine information across multiple frequencies \*/

4 Compute  $\widehat{\mathbf{V}}^{\max,t+1} \in \mathbb{R}^{N \times M}$ , whose  $(i, m)$ th entry satisfies

$$\widehat{\mathbf{V}}_{im}^{\max,t+1} \leftarrow \max_{\theta_i \in \Omega} \sum_{k=-K_{\max}}^{K_{\max}} \left\langle e^{\iota k \theta_i}, \widehat{\mathbf{V}}_{im}^{(k),t+1} \right\rangle \quad (23)$$

5 /\* Recovery of community memberships and associated phases \*/

For each node  $i \in [N]$ , assign its community membership as

$$\hat{\mathcal{M}}(i) \leftarrow \operatorname{argmax}_{m \in [M]} \widehat{\mathbf{H}}_{i,:}^{t+1}, \text{ where } \widehat{\mathbf{H}}^{t+1} \leftarrow \mathcal{P}_{\mathcal{H}}(\widehat{\mathbf{V}}^{\max,t+1})$$

then estimate the associated phase given the estimated community membership  $\hat{\mathcal{M}}(i)$

$$\hat{\theta}_i \leftarrow \operatorname{argmax}_{\theta_i \in \Omega} \sum_{k=-K_{\max}}^{K_{\max}} \left\langle e^{\iota k \theta_i}, \widehat{\mathbf{V}}_{i\hat{\mathcal{M}}(i)}^{(k),t+1} \right\rangle \quad (24)$$

6 Construct  $\{\widehat{\mathbf{V}}^{(k),t+1}\}_{k=-K_{\max}}^{K_{\max}}$  using  $\{\hat{\mathcal{M}}(i)\}_{i=1}^N$  and  $\{\hat{\theta}_i\}_{i=1}^N$  according to (12)

7 **end**

**Output:** Estimated community memberships  $\{\hat{\mathcal{M}}(i)\}_{i=1}^N$  and estimated phases  $\{\hat{\theta}_i\}_{i=1}^N$

---

estimation problem (23), which inspired by (17). The last step is estimating community memberships and associated phases. As mentioned before, giving  $\widehat{\mathbf{V}}^{\max,t+1}$  and then finding the corresponding community assignment is equal to solving the MCAP (see Definition 4). We need to project  $\widehat{\mathbf{V}}^{\max,t+1}$  onto the feasible set  $\mathcal{H}$  to obtain the matrix  $\widehat{\mathbf{H}}^{t+1}$  that indicates community memberships (line 5). The reason why the projection  $\mathcal{P}(\cdot)$  is chosen rather than directly using the index of largest entry in each row of  $\widehat{\mathbf{V}}^{\max,t+1}$  is because the latter one cannot guarantee the size of each community. The associated phases can be recovered according to the recovered community memberships (24). Besides, the modification of the iterative MF-GPM for the joint estimation problem with continuous phase angles is just the same as that of the spectral method based on the MF-CPQR factorization.

The iterative MF-GPM is originated from the classical power method (PM), which are used to compute the leading eigenvector. The only difference distinguish the iterative MF-GPM from PM is an additional projection onto the feasible set, which is induced by the constraints on  $\{\widehat{\mathbf{V}}^{(k),t}\}_{k=-K_{\max}}^{K_{\max}}$ . If we relax the constraints similar to (20), PM is capable of solving it. The motivation behind the proposed iterative MF-GPM is taking advantage of the efficiency of PM, as well as leveraging the information across multiple frequencies, to achieve better performance. In Section 6, numerical experiments show that iterative MF-GPM largely outperforms GPM (Chen et al., 2021).

## 5.2 Computational Complexity

In this section, we compute the complexity of Algorithm 4 step by step in Table 2. Again, here we assume  $M = \Theta(1)$ . In terms of initialization, the CPQR-type algorithm (Fan et al., 2021b) is  $\mathcal{O}(|\mathcal{E}|)$ . The matrix multiplication step consists of  $\mathcal{O}(K_{\max})$  times of matrix multiplication ( $\mathcal{O}(|\mathcal{E}|)$  per time). In order to combine information across multiple frequencies, we need to compute  $MN$  times of FFT of length- $K_{\max}$  vectors ( $\mathcal{O}(K_{\max} \log K_{\max})$  per

Table 2: The computational complexity of Algorithm 4 in each step, where both dense and sparse networks are included.

Steps	Computational Complexity
1. Initialization	$\mathcal{O}( \mathcal{E} )$
2. Matrix multiplication	$\mathcal{O}(K_{\max} \mathcal{E} )$
3. Combine information	$\mathcal{O}(NK_{\max} \log K_{\max})$
4. Estimate memberships and phases	$\mathcal{O}(N \log N)$
Total complexity	$\mathcal{O}(K_{\max} \mathcal{E}  + N \log N + NK_{\max} \log K_{\max})$

vector). For estimating community memberships and associated phases, we first need to project  $\widehat{\mathbf{V}}^{\max, t+1}$  onto  $\mathcal{H}$ , which is  $\mathcal{O}(N \log N)$ . Then complexity of estimating community memberships and associated phases using  $\widehat{\mathbf{H}}^{t+1}$  is negligible. When the network  $\mathcal{G}$  is densely connected with  $|\mathcal{E}| = \mathcal{O}(N^2)$ , Algorithm 4 ends up with  $\mathcal{O}(K_{\max}N^2)$  if  $N > \log K_{\max}$ . However, if  $|\mathcal{E}| = o(N^2)$ , for example  $\mathcal{O}(N \log N)$  and  $\mathcal{O}(N)$ , the complexity will be reduced to  $\mathcal{O}(K_{\max}N \max\{\log N, \log K_{\max}\})$  and  $\mathcal{O}(N \max\{\log N, K_{\max} \log K_{\max}\})$ , respectively. As a result, the computational complexity of Algorithm 4 is very similar to Algorithm 1.

## 6 Numerical Experiments

This section deals with numerical experiments of the spectral method based on the MF-CPQR factorization (Algorithm 1) and the iterative MF-GPM (Algorithm 4) to showcase their performance against state-of-the-art benchmark algorithms<sup>3</sup>. For comparison, the benchmark algorithms are chosen as i) the CPQR-type algorithm (Fan et al., 2021b), ii) the GPM (Chen et al., 2021), where both of them can be modified identically from the joint community and group synchronization problem into the joint community detection and phase synchronization problem. Specifically, algorithms in Fan et al. (2021b); Chen et al. (2021) are single frequency version of our proposed algorithms, which can be realized by replacing the summation over  $k$  in (17), (18), (23), and (24) with  $k = 1$ .

In each experiment, we generate the observation matrix  $\mathbf{A}$  using the probabilistic model, SBM-Ph, as discussed in Section 3 and estimate the community memberships and associated phase angles by the spectral algorithms based on the MF-CPQR factorization, the iterative MF-GPM, and the benchmark algorithms. To evaluate the numerical results, we defined two metrics, *success rate of exact recovery* and *error of phase synchronization*, for recovering the community memberships and associated phase angles. In terms of *success rate of exact recovery*, it shows the rate of algorithms exactly recover the community memberships. Let  $\hat{\mathcal{S}}_m = \{i \in [N] | \hat{\mathcal{M}}(i) = m\}$  be the set of nodes assigned into the  $m$ th community by algorithms, and we have that

$$\text{success rate of exact recovery} = \text{the rate } \{\hat{\mathcal{S}}_m\}_{m=1}^M \text{ is identical to } \{\mathcal{S}_m\}_{m=1}^M. \quad (25)$$

As for the *error of phase synchronization*, it assesses the performance of recovering phase angles. We define  $\boldsymbol{\theta}^{*,(m)} = [e^{i\theta_i^*}]_{i \in \mathcal{S}_m^*} \in \mathbb{C}^s$  for each community that concatenates the ground truth  $\theta_i^*$  for all  $i \in \mathcal{S}_m^*$ , and similarly  $\hat{\boldsymbol{\theta}}^{(m)} = [e^{i\hat{\theta}_i}]_{i \in \mathcal{S}_m^*} \in \mathbb{C}^s$  for the estimated phase angles. Then, after removing the ambiguity with aligning  $\hat{\boldsymbol{\theta}}^{(m)}$  with  $\boldsymbol{\theta}^{*,(m)}$  in each community as

$$\gamma^{(m)} = \underset{g^{(m)} \in \Omega \text{ or } [0, 2\pi]}{\operatorname{argmin}} \|\hat{\boldsymbol{\theta}}^{(m)} e^{ig^{(m)}} - \boldsymbol{\theta}^{*,(m)}\|_2, \quad \forall m = 1, \dots, M,$$

the *error of phase synchronization* is defined as

$$\text{error of phase synchronization} = \max_{m \in [M]} \max_{i \in \mathcal{S}_m^*} \{\min(|\hat{\theta}_i + \gamma^{(m)} - \theta_i^*|, 2\pi - |\hat{\theta}_i + \gamma^{(m)} - \theta_i^*|)\}. \quad (26)$$

The *error of phase synchronization* is actually the maximum error of estimated phase angles among all nodes. Besides, both the *error of phase synchronization* and *error of phase synchronization* are computed over 20 independent and identical realizations for each experiment in the following. In the rest of this section, we first present the results of the joint estimation problem in Section 6.1 and followed by the extension to continuous phase angles in Section 6.2.

<sup>3</sup>Codes are available in [https://github.com/LingdaWang/Joint\\_Community\\_Detection\\_and\\_Phase\\_Synchronization](https://github.com/LingdaWang/Joint_Community_Detection_and_Phase_Synchronization)

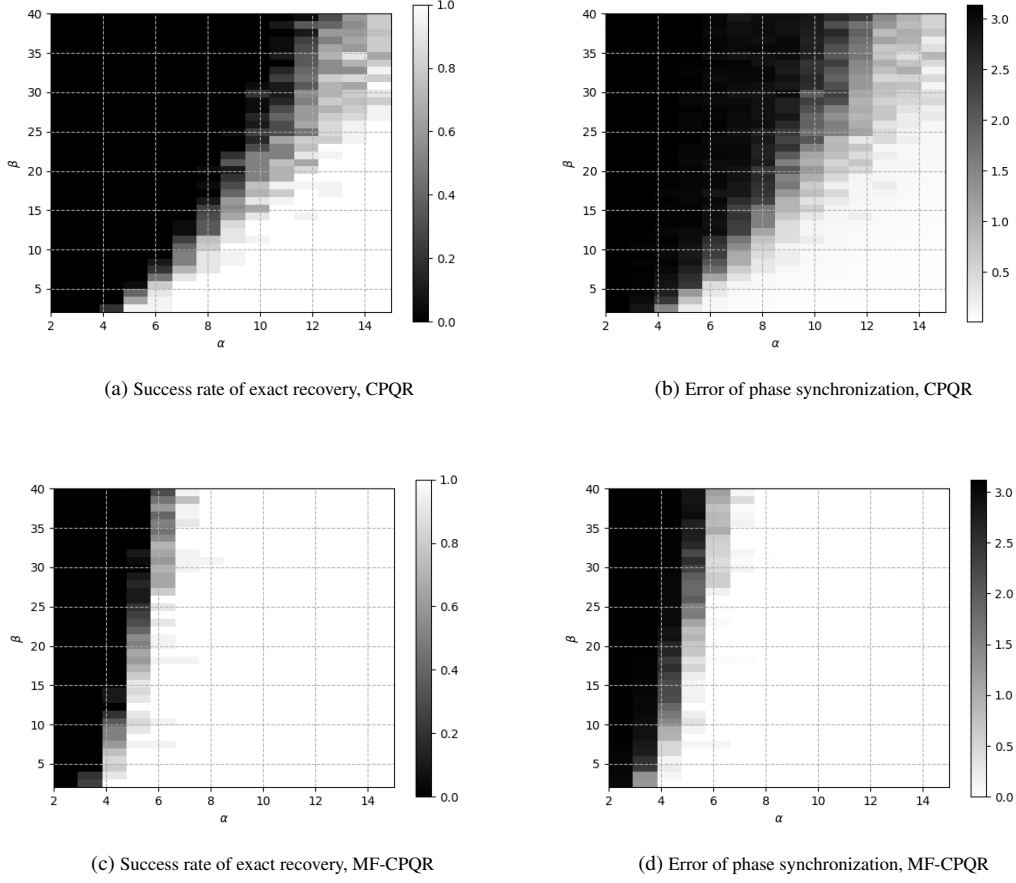


Figure 3: Results on two communities by the CPQR-type algorithm (Fan et al., 2021b) and the spectral method based on the MF-CPQR factorization. We conduct the experiment under the setting  $M = 2$ ,  $s = 500$  ( $N = 1000$ ), and  $K_{\max} = 16$ . (a) and (c): The success rate of exact recovery (25) under varying  $\alpha$  in  $p = \alpha \log n/n$  and  $\beta$  in  $q = \beta \log n/n$ ; (b) and (d): The error of phase synchronization (26) under varying  $\alpha$  and  $\beta$ .

## 6.1 Results of the Joint Estimation Problem

We first show the results of the spectral method based on the MF-CPQR factorization (Algorithm 1) against the CPQR-type algorithm (Fan et al., 2021b) on the joint estimation problem, where the case of  $M = 2$ ,  $s = 500$ , and  $K_{\max} = 16$  is considered. Similar to Fan et al. (2021b); Chen et al. (2021), we test the recovery performance in the regime  $p, q = \mathcal{O}(\log n/n)$ , where different  $p = \alpha \log n/n$  and  $q = \beta \log n/n$  with varying  $\alpha$  and  $\beta$  are included. In Figure 3, we show the *success rate of exact recovery* (25) and *error of phase synchronization* (26). As one can observe from Figure 3a and 3c, our proposed spectral method based on the MF-CPQR factorization outperforms the CPQR-type algorithm (Fan et al., 2021b) in the *success rate of exact recovery*. The *error of phase synchronization* follows a similar pattern.

Next, we test the performance of the iterative MF-GPM (Algorithm 4) against the GPM (Chen et al., 2021) under the same choice of  $M$ ,  $s$ , and  $K_{\max}$  as before. Since the GPM and the iterative MF-GPM require initialization that is close enough to the ground truth, we can choose either Chen et al. (2021, Algorithm 3) or the CPQR-type algorithm (Fan et al., 2021b). We set the number of iterations to be 50 as suggested by Chen et al. (2021). Again, as one can observe from Figure 4, our proposed iterative MF-GPM achieves higher accuracy in both the *success rate of exact recovery* and *error of phase synchronization*. Surprisingly, one may also notice the region where  $p$  is small and  $q$  is large (top left area in Figure 4c), the iterative MF-GPM is capable of recovering all community memberships

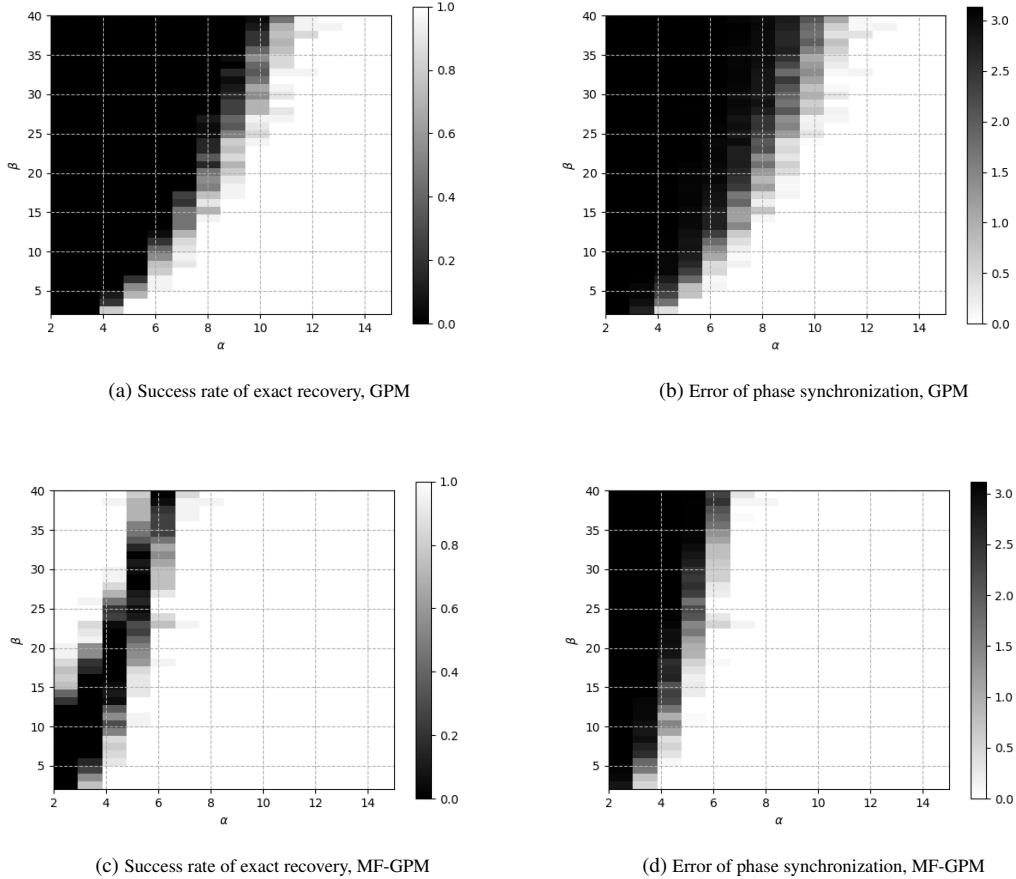


Figure 4: *Results on two communities by the GPM (Chen et al., 2021) and the iterative MF-GPM.* We conduct the experiment under the same setting as Figure 3. (a) and (c): The *success rate of exact recovery* (25) under varying  $\alpha$  in  $p = \alpha^{\log n}/n$  and  $\beta$  in  $q = \beta^{\log n}/n$ ; (b) and (d): The *error of phase synchronization* (26) under varying  $\alpha$  and  $\beta$ .

with high probability, however, this is not the case in recovering associated phase angles.

When compare the results shown in Figure 3 and 4 together, the spectral method based on the MF-CPQR factorization shows very similar result as the iterative MF-GPM, which are both much better than the GPM (Chen et al., 2021) and the CPQR-type algorithm (Fan et al., 2021b). However, compared to the iterative MF-GPM, the spectral method based on the MF-CPQR factorization is free of initialization. One may also observe the performance of the GPM (Chen et al., 2021) is better than the CPQR-type algorithm (Fan et al., 2021b).

## 6.2 Results with Continuous Phase Angles

In this section, we show the results of our proposed algorithms against benchmark algorithms on the joint estimation problem with continuous phase angles. As mentioned in Section 3.3, the algorithms tested in Section 6.1 can be directly applied after simple modification (See Section 4.1 for details), and thus we choose the similar setting as Section 6.1. Besides, since (15) is a truncated MLE formulation of the true one (13), experiments of the spectral method based on the MF-CPQR factorization and the iterative MF-GPM with different  $K_{\max}$  are conducted to study the trend of the results as  $K_{\max}$  grows. The results are detailed in Figure 5, with very similar performance as shown in Figure 3 and 4. In addition, as  $K_{\max}$  grows, the cluster membership identification and phase synchronization become more accurate in both MF-CPQR based method and iterative MF-GPM.

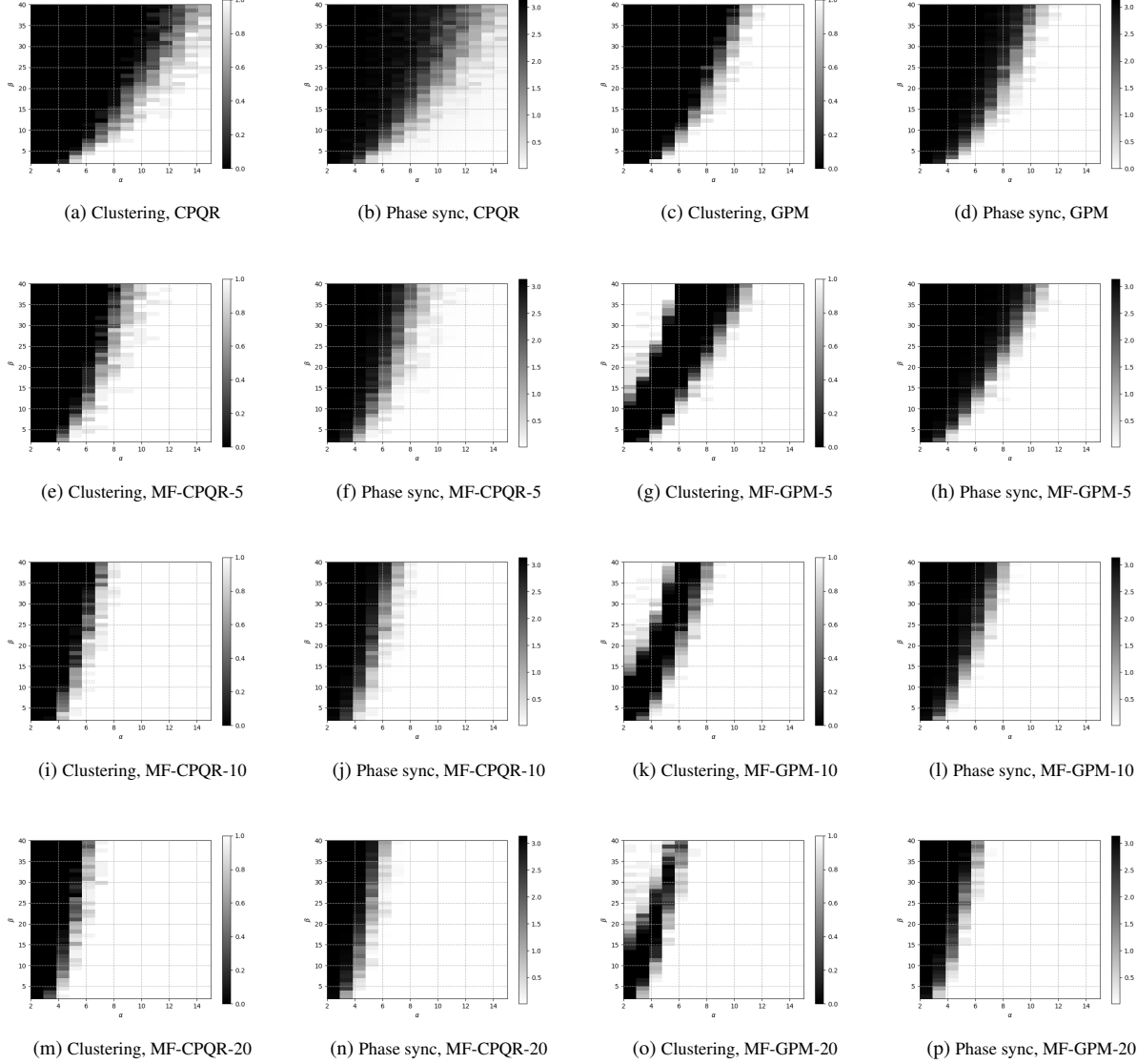


Figure 5: Results on joint clustering and phase synchronization with continuous phase angles in  $[0, 2\pi)$  by the CPQR-type algorithm (Fan et al., 2021b), the GPM (Chen et al., 2021), the spectral method based on the MF-CPQR factorization, and the iterative MF-GPM. The choice of  $M$  and  $s$  are the same as Figure 3. The first and third columns show the success rate of exact recovery (25), and the second and fourth columns shows the error of phase synchronization (26). (a), (b), (c), and (d): The results of the CPQR-type algorithm (Fan et al., 2021b), and the GPM (Chen et al., 2021); (e), (f), (g), and (h): The results of the spectral method based on the MF-CPQR factorization with  $K_{\max} = 5$ ; (i), (j), (k), and (l): The results of the spectral method based on the MF-CPQR factorization with  $K_{\max} = 10$ ; (m), (n), (o), and (p): The results of the spectral method based on the MF-CPQR factorization with  $K_{\max} = 20$ .

## 7 Conclusion

In this paper, we study the joint community detection and phase synchronization problem from an MLE perspective, and provide the new insight that its MLE formulation has a "multi-frequency" nature. We then propose two methods, the spectral method based on the novel MF-CPQR factorization and the iterative MF-GPM, to tackle the MLE

formulation of the joint estimation problem, where the latter one requires the initialization from spectral methods. Numerical experiments demonstrate the advantage of our proposed algorithms against state-of-the-art algorithms.

It remains open to establish the theoretical analysis that can tightly characterize the noise robustness of our proposed algorithms. Sub-optimal bounds can be easily derived following the analysis in (Fan et al., 2021b; Chen et al., 2021) by considering the frequency-1 component. However, these results do not explore additional frequency information. The key difficulties lie in i) analyzing the properties and relationships of eigenvectors among different frequency components with dependent noises, and ii) analyzing the power method across multiple frequencies. We leave them for future investigation.

In addition, there are several directions that can be further explored. It is natural to expect that the proposed approach can be extended to compact non-Abelian groups (e.g., rotational groups, orthogonal groups, and symmetric groups) using the corresponding irreducible representations.

## Acknowledgments

We would like to thank Dr. Xiuyuan Cheng and Yifeng Fan for helpful discussions. We also gratefully acknowledge the support from NSF grant DMS-1854791 and Alfred P. Sloan foundation.

## References

Abbe, E. (2017). Community detection and stochastic block models: Recent developments. *The Journal of Machine Learning Research*, 18(1):6446–6531.

Abbe, E., Bandeira, A. S., and Hall, G. (2015). Exact recovery in the stochastic block model. *IEEE Transactions on Information Theory*, 62(1):471–487.

Abbe, E., Fan, J., Wang, K., and Zhong, Y. (2020). Entrywise eigenvector analysis of random matrices with low expected rank. *The Annals of Statistics*, 48(3):1452.

Abbe, E. and Sandon, C. (2015). Community detection in general stochastic block models: Fundamental limits and efficient algorithms for recovery. In *2015 IEEE 56th Annual Symposium on Foundations of Computer Science*, pages 670–688. IEEE.

Amini, A. A. and Levina, E. (2018). On semidefinite relaxations for the block model. *The Annals of Statistics*, 46(1):149–179.

Bandeira, A. S. (2018). Random Laplacian matrices and convex relaxations. *Foundations of Computational Mathematics*, 18(2):345–379.

Bandeira, A. S., Boumal, N., and Singer, A. (2017). Tightness of the maximum likelihood semidefinite relaxation for angular synchronization. *Mathematical Programming*, 163(1):145–167.

Bandeira, A. S., Chen, Y., Lederman, R. R., and Singer, A. (2020). Non-unique games over compact groups and orientation estimation in cryo-EM. *Inverse Problems*, 36(6):064002.

Bandeira, A. S., Kennedy, C., and Singer, A. (2016). Approximating the little Grothendieck problem over the orthogonal and unitary groups. *Mathematical Programming*, 160(1):433–475.

Boumal, N. (2016). Nonconvex phase synchronization. *SIAM Journal on Optimization*, 26(4):2355–2377.

Bulirsch, R., Stoer, J., and Stoer, J. (1991). *Introduction to Numerical Analysis*. Springer.

Businger, P. and Golub, G. (1971). Linear least squares solutions by Householder transformations. In *Handbook for Automatic Computation*, pages 111–118. Springer.

Chaudhury, K. N., Khoo, Y., and Singer, A. (2015). Global registration of multiple point clouds using semidefinite programming. *SIAM Journal on Optimization*, 25(1):468–501.

Chen, S., Cheng, X., and So, A. M.-C. (2021). Non-convex joint community detection and group synchronization via generalized power method. *arXiv preprint arXiv:2112.14204*.

Chen, Y. and Goldsmith, A. J. (2014). Information recovery from pairwise measurements. In *2014 IEEE International Symposium on Information Theory*, pages 2012–2016. IEEE.

Chen, Z., Li, X., and Bruna, J. (2017). Supervised community detection with line graph neural networks. *arXiv preprint arXiv:1705.08415*.

Cucuringu, M., Singer, A., and Cowburn, D. (2012). Eigenvector synchronization, graph rigidity and the molecule problem. *Information and Inference: A Journal of the IMA*, 1(1):21–67.

Damle, A., Minden, V., and Ying, L. (2016). Robust and efficient multi-way spectral clustering. *arXiv preprint arXiv:1609.08251*.

Decelle, A., Krzakala, F., Moore, C., and Zdeborová, L. (2011). Asymptotic analysis of the stochastic block model for modular networks and its algorithmic applications. *Physical Review E*, 84(6):066106.

Fan, K. and Hoffman, A. J. (1955). Some metric inequalities in the space of matrices. *Proceedings of the American Mathematical Society*, 6(1):111–116.

Fan, Y., Khoo, Y., and Zhao, Z. (2021a). Joint community detection and rotational synchronization via semidefinite programming. *arXiv preprint arXiv:2105.06031*.

Fan, Y., Khoo, Y., and Zhao, Z. (2021b). A spectral method for joint community detection and orthogonal group synchronization. *arXiv preprint arXiv:2112.13199*.

Fei, Y. and Chen, Y. (2018). Exponential error rates of SDP for block models: Beyond Grothendieck’s inequality. *IEEE Transactions on Information Theory*, 65(1):551–571.

Frank, J. (2006). *Three-dimensional electron microscopy of macromolecular assemblies: Visualization of biological molecules in their native state*. Oxford university press.

Gao, T. and Zhao, Z. (2019). Multi-frequency phase synchronization. In *International Conference on Machine Learning*, pages 2132–2141. PMLR.

Girvan, M. and Newman, M. E. (2002). Community structure in social and biological networks. *Proceedings of the National Academy of Sciences*, 99(12):7821–7826.

Golub, G. H. and Van Loan, C. F. (1996). *Matrix Computations*. Baltimore, The Johns Hopkins University Press.

Guédon, O. and Vershynin, R. (2016). Community detection in sparse networks via Grothendieck’s inequality. *Probability Theory and Related Fields*, 165(3):1025–1049.

Hajek, B., Wu, Y., and Xu, J. (2016a). Achieving exact cluster recovery threshold via semidefinite programming. *IEEE Transactions on Information Theory*, 62(5):2788–2797.

Hajek, B., Wu, Y., and Xu, J. (2016b). Achieving exact cluster recovery threshold via semidefinite programming: Extensions. *IEEE Transactions on Information Theory*, 62(10):5918–5937.

Krzakala, F., Moore, C., Mossel, E., Neeman, J., Sly, A., Zdeborová, L., and Zhang, P. (2013). Spectral redemption in clustering sparse networks. *Proceedings of the National Academy of Sciences*, 110(52):20935–20940.

Leskovec, J., Lang, K. J., Dasgupta, A., and Mahoney, M. W. (2008). Statistical properties of community structure in large social and information networks. In *Proceedings of the 17th International Conference on World Wide Web*, pages 695–704.

Li, X., Chen, Y., and Xu, J. (2021). Convex relaxation methods for community detection. *Statistical Science*, 36(1):2–15.

Liu, H., Yue, M.-C., and Man-Cho So, A. (2017). On the estimation performance and convergence rate of the generalized power method for phase synchronization. *SIAM Journal on Optimization*, 27(4):2426–2446.

Massoulié, L. (2014). Community detection thresholds and the weak Ramanujan property. In *Proceedings of the 46th Annual ACM Symposium on Theory of Computing*, pages 694–703.

McSherry, F. (2001). Spectral partitioning of random graphs. In *Proceedings 42nd IEEE Symposium on Foundations of Computer Science*, pages 529–537. IEEE.

Ng, A., Jordan, M., and Weiss, Y. (2001). On spectral clustering: Analysis and an algorithm. *Advances in Neural Information Processing Systems*, 14.

Perry, A. and Wein, A. S. (2017). A semidefinite program for unbalanced multisecision in the stochastic block model. In *2017 International Conference on Sampling Theory and Applications (SampTA)*, pages 64–67. IEEE.

Perry, A., Wein, A. S., Bandeira, A. S., and Moitra, A. (2018). Message-passing algorithms for synchronization problems over compact groups. *Communications on Pure and Applied Mathematics*, 71(11):2275–2322.

Singer, A. (2011). Angular synchronization by eigenvectors and semidefinite programming. *Applied and Computational Harmonic Analysis*, 30(1):20–36.

Singer, A., Zhao, Z., Shkolnisky, Y., and Hadani, R. (2011). Viewing angle classification of cryo-electron microscopy images using eigenvectors. *SIAM Journal on Imaging Sciences*, 4(2):723–759.

Stewart, G. W. (2002). A Krylov–Schur algorithm for large eigenproblems. *SIAM Journal on Matrix Analysis and Applications*, 23(3):601–614.

Su, L., Wang, W., and Zhang, Y. (2019). Strong consistency of spectral clustering for stochastic block models. *IEEE Transactions on Information Theory*, 66(1):324–338.

Tokuyama, T. and Nakano, J. (1995). Geometric algorithms for the minimum cost assignment problem. *Random Structures & Algorithms*, 6(4):393–406.

Trefethen, L. N. and Bau III, D. (1997). *Numerical Linear Algebra*, volume 50. SIAM.

Vu, V. (2018). A simple SVD algorithm for finding hidden partitions. *Combinatorics, Probability and Computing*, 27(1):124–140.

Wang, P., Liu, H., Zhou, Z., and So, A. M.-C. (2021). Optimal non-convex exact recovery in stochastic block model via projected power method. *arXiv preprint arXiv:2106.05644*.

Yun, S.-Y. and Proutiere, A. (2014). Accurate community detection in the stochastic block model via spectral algorithms. *arXiv preprint arXiv:1412.7335*.

Zhang, S. and Huang, Y. (2006). Complex quadratic optimization and semidefinite programming. *SIAM Journal on Optimization*, 16(3):871–890.

Zhao, Z. and Singer, A. (2014). Rotationally invariant image representation for viewing direction classification in cryo-EM. *Journal of Structural Biology*, 186(1):153–166.

Zhong, Y. and Boumal, N. (2018). Near-optimal bounds for phase synchronization. *SIAM Journal on Optimization*, 28(2):989–1016.